PLASMA BETA ABOVE A SOLAR ACTIVE REGION: RETHINKING THE PARADIGM

G. ALLEN GARY
Marshall Space Flight Center, Huntsville, AL 35812, U.S.A. (e-mail: Allen.Gary@msfc.nasa.gov)

(Received 23 March 2001; accepted 16 July 2001)

Abstract. In this paper, we present a model of the plasma beta above an active region and discuss its consequences in terms of coronal magnetic field modeling. The β-plasma model is representative and derived from a collection of sources. The resulting β variation with height in the solar atmosphere is used to emphasize that the assumption that the magnetic pressure dominates over the plasma pressure must be carefully employed when extrapolating the magnetic field. This paper points out (1) that the paradigm that the coronal magnetic field can be constructed from a force-free magnetic field must be used in the correct context, since the force-free region is sandwiched between two regions which have $\beta > 1$, (2) that the chromospheric Mg II–C IV magnetic measurements occur near the β-minimum, and (3) that, moving from the photosphere upwards, β can return to ~ 1 at relatively low coronal heights, e.g., $R \sim 1.2\ R_s$.

1. Introduction: Plasma Beta

The structure of the solar atmosphere is a complex plasma in which magnetic and plasma pressure play interchanging roles for dominance. The dominating force is described by the plasma β, which is the ratio of gas pressure to magnetic pressure, $(8\pi p/B^2)$. When $\beta > 1$, then the gas pressure dominates over the magnetic pressure. As a function along a magnetic field line, this ratio might vary from $\beta > 1$ in the photosphere at the base of the field lines, to $\beta \ll 1$ in the mid-corona, to $\beta > 1$ in the upper corona. Most current magnetic field extrapolations do not or cannot take into account the *full* range of β. They essentially assume $\beta \ll 1$, since the full boundary conditions do not exist in the *two* $\beta > 1$ regions. The prevalence of the use of force-free magnetic fields in extrapolating the coronal field can be considered a paradigm. In this paper we point out that this paradigm should be reconsidered since the region of $\beta < 1$ is limited. Historically, spherical magnetic potential models have been introduced which hide the β-variation within an imaginary, thin source surface (which is approximately where the dynamic pressure equals the magnetic pressure) (Schatten, Wilcox, and Ness, 1969). These solutions completely neglect the *extended* influence of the solar wind, which starts to drag and distort the magnetic field at relatively low heights (Altschuler and Newkirk, 1969). Although it has been known that β becomes $\gtrsim 1$ in the range of $\sim 2\ R_s$, its high values at lower heights have not been generally recognized. In this paper, we present a model of β as a function height to emphasize its variations in the mid-

Solar Physics **203:** 71–86, 2001.
© 2001 *Kluwer Academic Publishers. Printed in the Netherlands.*

corona. In the upper corona and the super-corona where $\beta \sim 1$, there are numerous coronal models which include gravity, gas pressure, field-aligned currents, and cross-field currents, however there are none that actually extrapolate the magnetic field upward through an active region over the three regions of β without making very special assumptions. The work by Zhao and Hoeksema (1994) and Neukirch (1995) come close, but the first introduces an artificial cusp surface and the second contains special solutions.

Generally, the plasma β is greater than one at the photosphere and less than one in the mid-corona. The plasma β is defined with scaled parameters by

$$\beta = \frac{\text{plasma pressure}}{\text{magnetic pressure}} = 16\pi\xi n K_B T/B^2 \simeq 0.07\ \xi\ n_9 T_6/B_1^2, \tag{1}$$

where $\xi = 1$ (1/2) for the corona (photosphere), $K_B = 10^{-15.86}$ erg deg^{-1}, $B_1 = B/10$, $n_9 = n/10^9$, and $T_6 = T/10^6$. For the photosphere where $\tau = 0.01$ ($h \simeq$ 250 km, $p = 1.25 \times 10^4$ dyn cm^{-2}) with typical values of $B = 500$ G, $n = 2 \times 10^{17}$ cm^{-3}, and $T = 5 \times 10^3$ K; the value for β is high, $\beta = 14$. For coronal values of $B = 10$ G, $n = 1.0 \times 10^9$ cm^{-3}, and $T = 3 \times 10^6$ K ($P = 0.83$ dyn cm^{-2}, $h \sim 10^2$ Mm), one obtains $\beta = 0.2$. We see that this coronal β value is not much less than one and we shall show that β is not everywhere less than one in the mid-corona as it is sometimes assumed. (The related parameters of these two examples are marked by diamond symbols in Figures 1, 2, and 3.) We shall now show the motivation for developing the β model and the develop a simple model to describe the β variation with height.

2. Development of the Model

There is ample evidence to suggest that β is > 1 at relatively low coronal heights. For example, the β values derived from SXT limb observations by Gary and Alexander (1999) have values approaching one (these results are labeled as 'SXT limb data' in the β-model of Figure 3). Hence for heights of 0.2–0.3 R_s the gas pressure again becomes important. Furthermore, the necessary radial stretching needed to match the field lines with the SXT observations for the AR 7999 implies that gas pressure is significant at a relatively low coronal height (Gary and Alexander, 1999). The observed SXT images of cusp indicate that the magnetic field has a y-type magnetic topology or a slowly moving x-point that is being produced in a region of high beta (e.g., see Suess, Gary, and Nerney, 2000) since a null or a current sheet has been formed. The many direct SXR images of cusped loops also imply that $\beta > 1$ occurs frequently in relatively low-lying regions (Hiei and Hundhausen, 1996; Strong, 1994). Two examples of SXT/*Yohkoh* cusp images on the limb are shown in Figure 4, where the cusp of panel A is associated with the AR 7008 and Figure 4(b) is associated with an older dispersed active region. For two more additional examples which are seen on the disk by SXT one can refer to

cusps of AR 8038 (12 May 1997) and AR 8071 (12 Aug 1997); however, seen at an acute angle their heights cannot be determined as readily. These SXT cusps are interpreted within the standard magnetic eruption models to represent reconnection sites as a current sheet with open field lines above the cusp (e.g., Moore *et al.*, 2001; Yokoyama *et al.*, 2001; McKenzie and Hudson, 1999). These open field lines are analogous to open field lines associated with the coronal streamers. Suess, Gary, and Nerney (2000) point out that β is > 1 in streamers from UVCS/SOHO observations and that β is ~ 20 at a height of 0.6 R_s using early MHD models by Pneuman and Kopp (1971). We assume that these active region cusps are associated with a magnetic field that is dominated by two strong opposite polarity flux regions and by symmetry arguments, for the dipolar field, there is no perpendicular field component to the symmetry line. Hence, directly above the cusp point, there is a weak magnetic field region where the anti-parallel field lines cancels and a current sheet exist and gas pressure dominates. Outside and above the cusp, the open field, dominated by the solar wind outflow, expands since its not connected in a closed loop and the resulting field is weak. In the near-photospheric region, the importance in which β is > 1 has also been considered recently. Berton's (2000) method to extrapolate quasi-force-free fields requires that the $\beta > 1$ region at the photosphere must be taken into account. Hence modeling the coronal field must consider the importance of gas pressure ($\beta > 1$) at both the lower and upper boundaries. In the following development of the pressure and magnetic models we do not intend to give a complete survey but only need to have generally consistent models that allow the derivation of the general nature of the plasma β dependency with height. In Sections 2.1 and 2.2, the magnetic field and pressure models which we employ are described and through a discussion of (i) the observational constraints, (ii) a empirical mathematical formulation, and (iii) a comparison of the mathematical curve with the observations. In Section 2.3, the β model is derived and discussed.

2.1. MAGNETIC MODEL

2.1.1. *Observational Constraints of the Field*

The height dependence of the magnetic field is observationally a difficult problem since there are few visible observations of chromospheric–coronal Zeeman lines and, in general, even though there are very good non-LTE radiative transfer theories for the these lines, their formation height is ambiguous due to the solar dynamics. On the other hand, the photospheric magnetic field is regularly obtained with the Fe I 630.2, Fe I 525.0 nm, and Fe I 868.8 nm lines which have typical formation heights of 200–300 km (Bruls, Lites, and Murphy, 1991). (These measurements still have some problems, but these problems concern the detailed interpretations of asymmetric Stokes line profiles, which probably result from the details of magnetic gradients and flows. However, the direct measurement of visible and IR Zeeman splittings provides a check that the stronger magnetic field strength measurements are within 20% of the true field strength.)

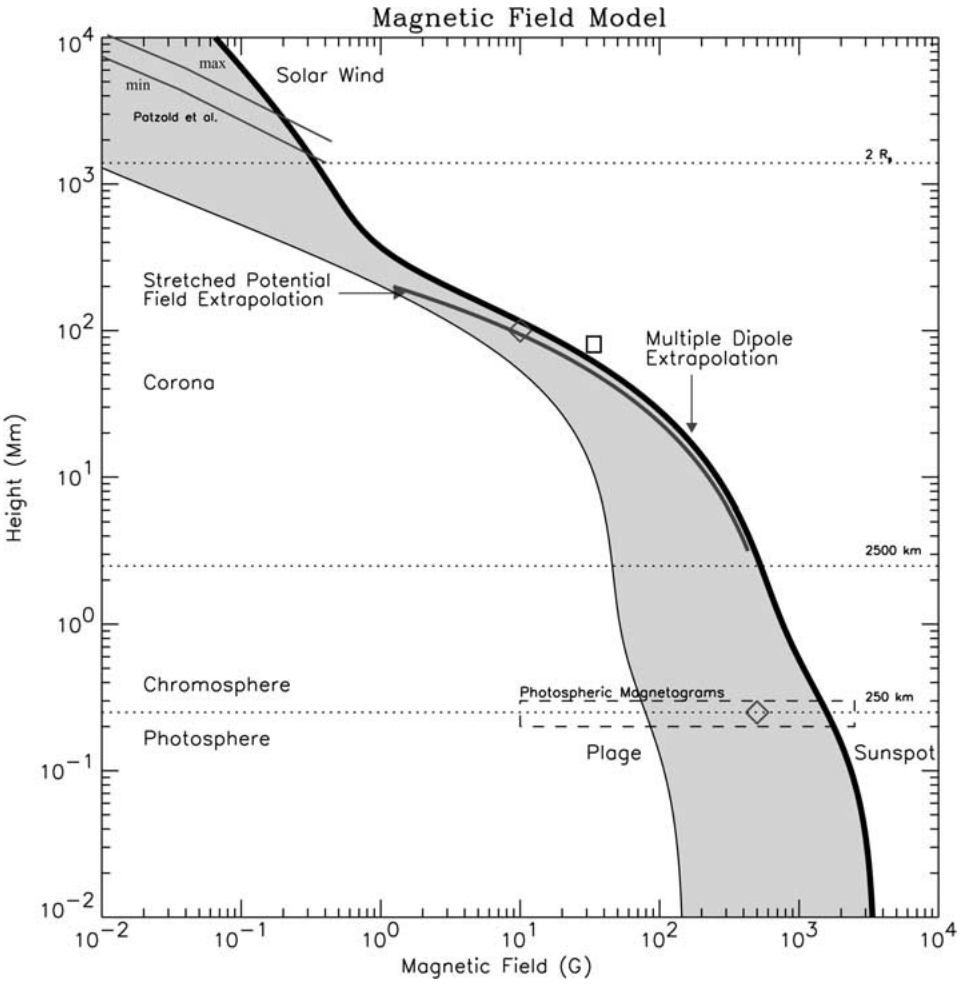

Figure 1. Magnetic field model over an active region. The magnetic field intensity as a function of height is shown shaded for open and closed field lines originating between a sunspot of 2500 G and a plage region of 150 G. The photospheric level of 250 km, the chromospheric level of 2500 m, and the coronal level of 2 R_s (2 solar radii) are shown as *horizontal dotted lines*. The *diamond symbols* mark the photospheric and coronal example points used in the text. The stretched potential field extrapolation is derived by radially stretching the potential field to match the coronal SXT loops (Gary and Alexander, 1999).

There is very little clear information about the magnetic field strength above active regions in the chromosphere and corona. In the wings of NaD lines the height of formation is 600 km, which is a couple of pressure scale heights above the Fe I lines height. This data indicates an umbra-penumbral magnetic gradient of 0.8–1.1 G km^{-1} (Metcalf *et al.*, 1995). Hagyard *et al.* (1983) report gradients of 0.11–0.36 G km^{-1} using the C IV 154.8 nm observations in conjunction with Fe I 525.0 nm with comparison values of 0.21 and 0.16 G km^{-1} from gradients

derived from the transverse photospheric measurements and the potential field, respectively. These linear gradients are not useful to infer the coronal field in that the valid range is only 1 Mm. Harvey (1969) obtained an exponential gradient of 1.6 G km^{-1} from prominence observations (which is compatible with the slope in Figure 1 in the chromosphere–low corona region for $H < 10^1$ Mm). The chromospheric Ca II and Mg II observations have been scattered and the non-LTE inversion requirements, the anomalous profiles, and the relatively low height of formation have limited their use in defining the mid-coronal magnetic field (Socas-Navarro, Trujillo Bueno, and Ruiz Cobo, 2000). Above an active region, using the coronal line Fe XIII 1074.7 nm, (Lin, Penn, and Tomczyk, 2000), obtained off-limb magnetic field strengths of 10 and 33 G at heights of 100 and 80 Mm, respectively. Their point (10 G, 100 Mm) coincides with the upper diamond symbol in Figure 1, and the box symbol represents their other point. The limited number of coronal magnetic field measurements above active regions should be taken with precaution due to the difficulty of the measurements. These integrated line-of-sight field strengths represent a lower limit to the total field strength. With these provisos, these data are used here to give credence to the modified potential extrapolation that we have used in the model. There have been magnetic field measurements in prominences, but they give no indication of how the magnetic field varies with height above active regions.

From 2 to 15 solar radii, Pätzold *et al.* (1987) obtained from Faraday rotation the global magnetic field variation of $B = (6/R^3 + 1.18/R^2)$ G with R in solar radii R_s (which is compatible with Figure 1 in the region for $H > 2R_s$ for solar maximum (max) and minimum (min)). We use their results, not to imply the multipole field configuration, but to provide a model for the magnetic field variation with height (Figure 1). Their line-of-sight Faraday rotation provides a unique measurement given their electron density function and assuming that the field is basically perpendicular to the line of sight. Their resulting values are consistent with the earlier plots of the magnetic field in this height range as given by Dulk and McLean (1978).

The magnetic field values derived from microwave gyro-resonant observations have height uncertainties. The specific height above the photosphere at which the coronal measurements are made remains an uncertainty (Lee *et al.*, 1997) but the gyro-resonant measurements are generally consistent with potential field extrapolations. Within the range of $H = 10^1$–10^3 Mm ($\sim$ 1–2 R_s), the standard method to derive the height dependence of the field remains the potential field extrapolation (Gary and Alexander, 1999; Aschwanden *et al.*, 1999). The introduction of electric current-carrying field lines produces little alteration. McClymont and Mikić (1994) have used a 3D resistive MHD code to model an active region and have found the field lines carrying the largest electric currents (the most non-potential field lines) produce expansion factors of less than 1.33 as compared to a potential field. Also since the non-potential magnetic field component (i.e., the free-energy component) is less than 10% as indicated by the amount of energy released in flares, it is

assumed here that a modified potential field adequately describes the field in the mid-coronal regions in terms of the *height dependency*. We assume this because the release of this energy in large flares sets the approximate value of the non-potential component of the magnetic field. The radially stretched fields provide electric currents that are comparable with non-potential active regions (Gary and Alexander, 1999). We use this set of data and models to estimate the final magnetic model used in the β calculation. The exact determination of the coronal field awaits scientific improvements in instrumentation and analysis.

2.1.2. *Mathematical Formulation*

The static model we use for the magnetic field starts by defining the upper magnetic envelope of a set of stretched potential lines for an active region (Gary and Alexander, 1999; Aschwanden *et al.*, 1999). A point on the envelope gives the maximum field strength at a given height. The equation of the envelope is defined by a set of parametric dipole terms in order to map out the height dependency (Aschwanden *et al.*, 1999). These terms are not intended to have a strict physical meaning but are used to derive an expression for the magnetic field variation. The final form of the equation for the upper envelope defining the field above the umbra is given by

$$B = B_s/(1 + H/H_s)^3 + B_f/(1 + H/H_f)^3 + B_w/(1 + H/H_w)^3, \quad (2)$$

where H_s, H_f, and H_w are the mean dipole depths, 0.5, 75, and 696 Mm and B_f, B_s, and B_w are 2500, 50, and 1 G, respectively. The equation is a parametric formulation to allow the following constraints to be satisfied: (1) The strong field model had to capture the magnetic field extrapolation by Gary and Alexander (1999) in the mid-corona since these generated field lines agree with the mid-corona structures which effectively accounts for the upper boundary conditions. To satisfy this requirement the middle dipole adopts the mean dipole depth of Aschwanden *et al.* (1999) (75 Mm) and a mean value of 50. (2) A photospheric umbra field strength of 2500 G was imposed which represents a typical umbra strength (e.g., Kopp and Rabin, 1992). This requirement was set by the umbra mean value with the mean dipole depth set to have minimum influence on the first requirement. (3) A correction for the solar wind was included such that the field decay was consistent with the outer coronal estimates (Pätzold *et al.*, 1987). This solar wind correction was imposed to simulate the observed magnetic field strength decay in the region above $2R_s$. Between 10^2 and 10^3 Mm the magnetic field of a single active region merges into a global field which is dominated in our model by a large dipole field. The three quasi-physical terms are related to the dipole of the strong umbral fields, the dipole of the overall active region, and the dipole of the sun. The first term, the strong umbral field dipole, decays rapidly due to the expansion of the field, and the third term is adjusted to correct for the stretching of the field due to the outflow of solar wind. Similarly, a lower envelope for the magnetic field above a plage was generated by using the same depth values for H_s, H_f, and H_w and 100, 50, and 0.005 G for B_f, B_s, and B_w, respectively. The two envelopes form the boundaries

of the shaded region in Figure 1. Below 0.025 Mm, the model does not take into account the collapsing of the field into strong flux tubes (Rabin, 1991; Rüedi *et al.*, 1992).

2.1.3. *Comparison of Model with Data*

The variation of the magnetic field to a height of 10^4 Mm ($\sim$ 14 R_s) above a plage and umbral sunspot region is shown in Figure 1, with the photospheric, chromospheric, and upper coronal boundaries indicated by horizontal dotted lines at 0.250, 2.50, and 1392 Mm (e.g., 250 km, 2500 km, and 2 R_s). The magnetic field in the region is consistent with the observational constraints listed above. The two diamonds are the values of the magnetic field and height used in the introductory photospheric and chromospheric examples for β. The stretched potential curve for magnetic field strength derived by Gary and Alexander (1999) for an active region is shown. The stretched potential field was calculated without imposing an extended source surface and hence is not expected to be representative above the observed loops (i.e., at $\sim 2\ R_s$). This curve was derived to represent the maximum magnetic field to a height of 3×10^2 Mm. Above this height, a correction term for the solar wind effect of radically stretching out the magnetic was introduced to be consistent with the higher coronal magnetic field data. A field correction at relatively low heights is obviously needed to have the low cusps as seen in the SXT/*Yohkoh* data (Figure 4). Both cusps of Figure 4 appeared quasi-static and remain distinct cusps for over 24 hours and are not just a short-time eruptive phenomenon. They require $\beta > 1$ for an extended period of time. Though not considered here, the variation of β with height also may have a time dependency.

2.2. PRESSURE MODEL

2.2.1. *Observational Constraints of the Gas Pressure*

The observational constraints of the pressure are categorized by a combination of semi-empirical fits of various chromospheric non-LTE radiative transfer calculations and of an isothermal coronal at $T = 1.4$ MK. The series of non-LTE radiative models plotted in Figure 2 are the quiet-Sun A-F VAL models of Vernazza, Avrett, and Loesner (1981) and the heated FAL-3 model of Fontenla, Avrett, and Loesner (1999) (dotted curve at the far right). We use these to summarize the observations of the chromosphere. In the mid-corona the major constraints used are the pressure results from Gary and Alexander (1999) which they derived from *Yohkoh*/SXT observation above an active region on the limb. These measurements assumed a integration length of $10^{4.4}$ km which gives a filling factor of 0.2 taking into account the size of the active region. The density is derived from integrated limb observations through the loops structure of the active region, hence is more representative of the pressure above the center of the active region (cf., Yoshida and Tsuneta, 1996), where the filling factor would have to approach unit for the pressure to represent the average pressure. As a reality check, two pairs of pressure curves derived

from loop models are shown in Figure 2. These are labeled 'RTV models' and 'SXT Loop Data', which refer to the pressures which are derived from the apex heating RTV models (Rosner, Tucker, and Vaiana, 1978, Equation (4.3) and a best-fit of coronal SXT/*Yohkoh* observations by Kano and Tsuneta (KT, 1995, Equation (19)), respectively. These models assume (i) the constant pressure of the loops is related to the mean coronal pressure at the apex height H of the loops, (ii) the loop pressure is $p \sim T^x/H$ ($x = 3$ for RTV and 5.1 for KT) and (iii) the temperature is constant (and in Figure 2, a temperature of 1 and 3 MK are used to generate two curves for each model), and (iv) the height is related to the loop length. For the upper coronal region the smoothed coronal electron density $n(H)$ as a function of height (Allen, 1973) is used to plot two pressure curves ($p = 2n(H)K_BT$) at $T = 1$ and 3 MK.

2.2.2. *Mathematical Formulation*

Our pressure model is formulated using two barometric terms representing the different temperature regions. The equation is

$$p(H) = p_c e^{-(H/H_c)(R/R_s)} + p_k\, e^{-(H/H_k)(R/R_s)}, \tag{3}$$

where $R = R_s + H$ and $H_c = H_o(R/R_s)^2$. Here H_c is the effective coronal scale height corrected for gravity, and H_k is the chromospheric scale height. The parameters have the values $p_c = 1.5$ dyn cm^{-2}, $p_k = 1 \times 10^5$ dyn cm^{-2}, $H_o = 55$ Mm, and $H_k = 0.12$ Mm. At 250 km, p was set to 1.25×10^4 dyn cm^{-2}. The coronal barometric model was selected to contain the Gary and Alexander (1999) pressure data and fit the Allen (1973) N_e data at 2.5×10^3 Mm for $T = 2$ MK.

2.2.3. *Comparison of Model with Data*

The model approximates the FAL3 model in the chromosphere and the Gary and Alexander–*Yohkoh*/SXT derived pressures in the middle coronal. The pressure results of Gary and Alexander are influenced, in part, by the brightest loops; this effect has been neglected here. The densities measured in the mid-corona have an unknown filling factor. The calculation by Gary and Alexander assumed an integration path length of $10^{4.4}$ km. Their active region size was factor 5 times this giving an estimated filling factor of 0.2. For active regions a filling factor of 0.1–0.2 is appropriate. The densities associated with an active region are higher than the global densities and hence associated pressures are reflected in Figure 2 (e.g., see Yoshida and Tsuneta, 1996, where the filling factor is ~ 0.15). Because our model has only two components it gives a rougher approximation to the upper corona pressures derived from the isothermal models. Overall the resulting curve gives a good representation over the region of interest. The upper limit of the gray shadowed region is an extension of a factor of 10 above our pressure model in the chromosphere–corona to account for over pressures of non-steady-state loops (Aschwanden, Schrijver, and Alexander, 2001; Aschwanden *et al.*, 1999) and high-temperature SXT loops (Yoshida and Tsuneta, 1996).

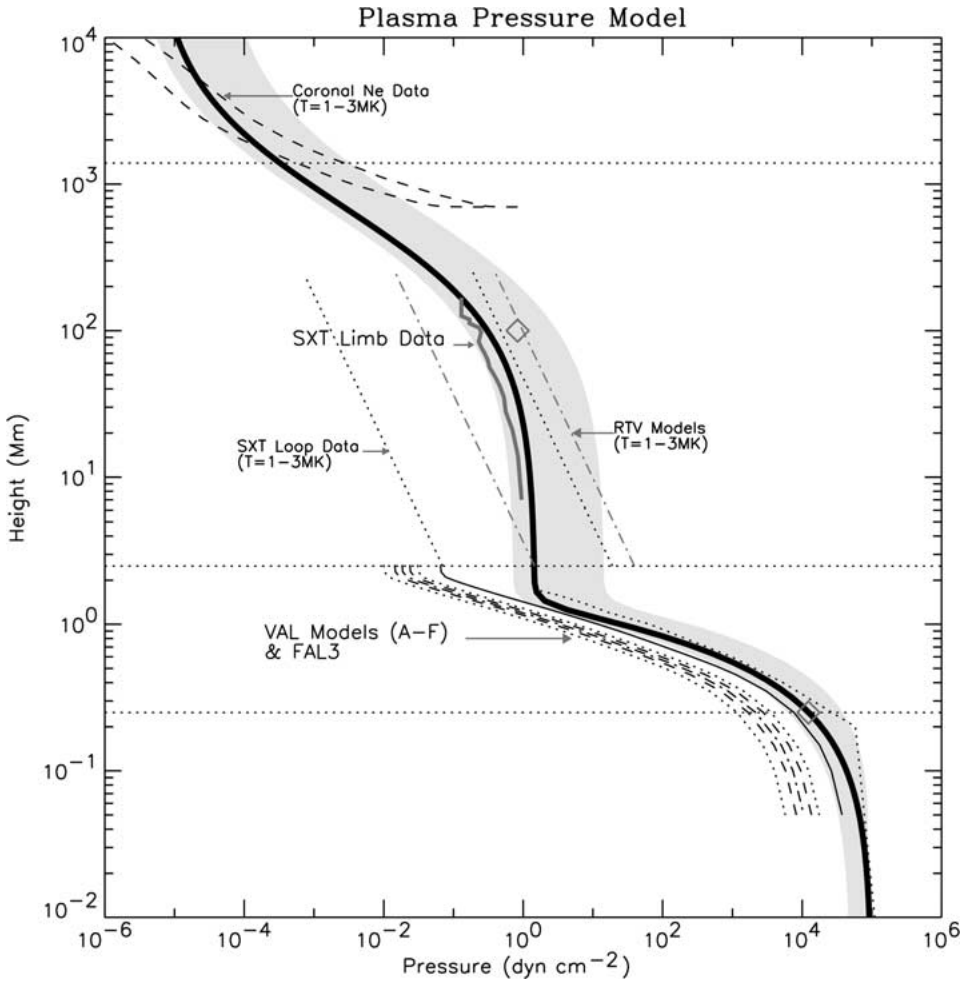

Figure 2. Plasma pressure model over an active region as shown by the *heavy solid line* with a gray shadow. The chromospheric pressure data has been summarized by the use of the VAL and FAL3 models (*broken pattern lines*). The mid-corona pressure for the model agrees with the derived pressure using *Yohkoh*/SXT limb data (Gary and Alexander, 1999) (*solid short line*). Various loop model dependencies are shown for comparison. For comparison, at $R_s \sim 2$, two isothermal models ($T = 1$ and 3 MK) are shown which employ observed coronal electron density (N_e) data. They only roughly influence the derived two-component model. The upper limit of the gray shadow represents pressures of hotter loops.

2.3. RESULTING BETA MODEL

The resulting model for β as derived from the ratio of plasma pressure to magnetic pressure is given in the curve of Figure 3. For simplicity of representation in the final β model, only a single pressure model has been used in deriving β. The higher pressures of very hot or non-steady state loops, which represent pressure inside

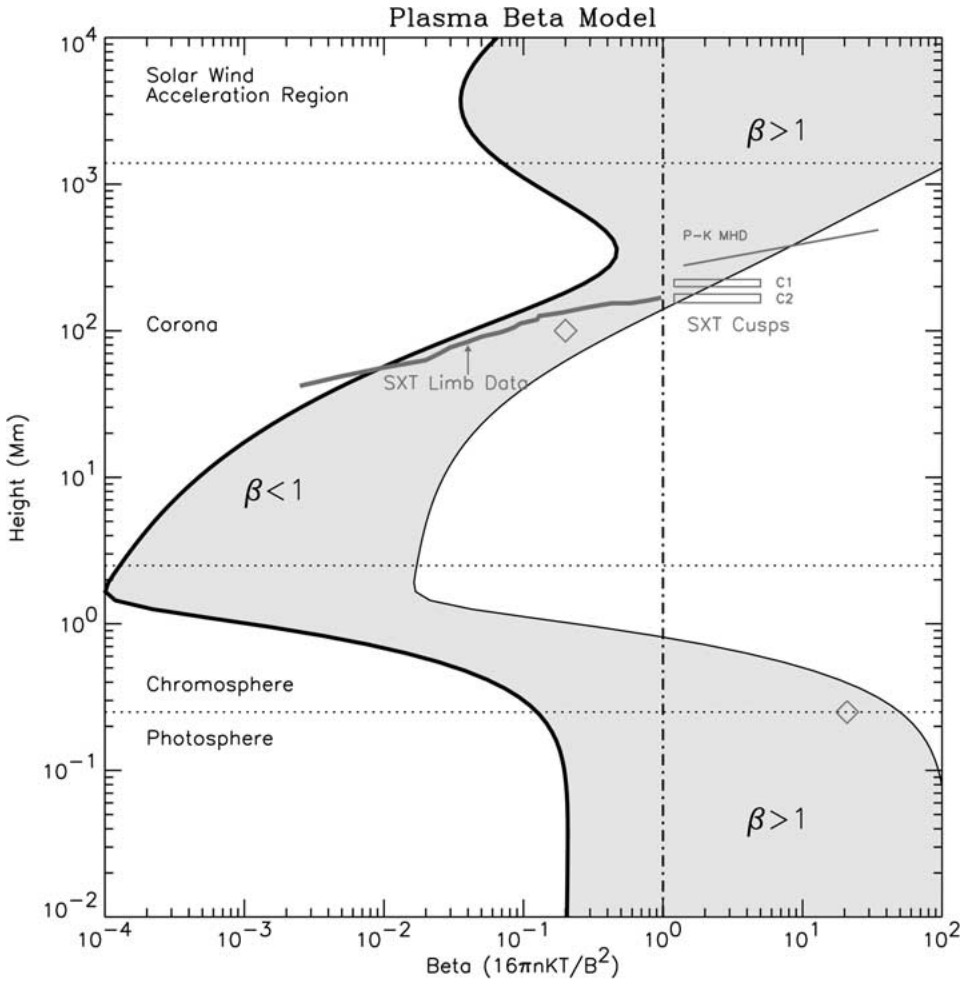

Figure 3. Plasma beta model over an active region. The plasma beta as a function of height is shown shaded for open and closed field lines originating between a sunspot of 2500 G and a plage region of 150 G. (The plage curve can also represent older, decaying active regions that have no umbral features.) The *diamond symbols* mark the photospheric and coronal example points used in the text. Various data indicate that β approaches unity at relatively low heights in the mid-corona as explained in the text.

selected flux tubes, are not used. Using these pressures would increase β and would have β reaching unity lower in the corona. The two side boundaries of the shaded regions in the β model are generated by the plage and umbra magnetic models of Figure 1. For very strong magnetic fields above the umbra the plasma-β remains less than unity but $\beta > 0.1$ near the photosphere and at the upper corona. However, outside these umbra regions in the plage regions representing most of an active region, the plasma-β is > 1 at the photosphere and in the upper corona. In the

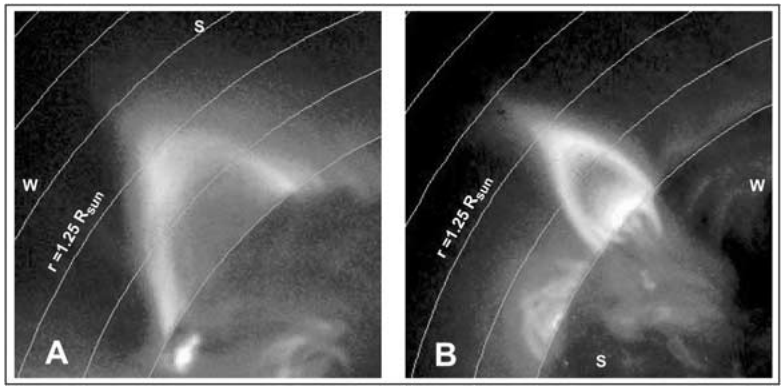

Figure 4. Two cusped loops (C1 and C2) observed by SXT/*Yohkoh* are shown at the west limb on 24 January 1992 (rotated, A) and the east limb on 18 March 1999 (B). The cusps are at a height of $r = 0.23\ R_s$ and $r = 0.25\ R_s$. The pressure and inertial forces of the solar wind dominate over the magnetic forces at the cusp and distend the field outwards. This implies $\beta \gtrsim 1$ at these heights. The heights of these SXT cusps are located well below the classical source surface height (see Figure 1).

chromosphere β reaches a minimum close to the photosphere at ~ 2 Mm with $\beta < 3 \times 10^{-2}$.

2.3.1. *Comparison with Data*

For comparison, data points have been added to Figure 3. Since the SXT limb data of Gary and Alexander (1999) was used to derive the magnetic and pressure model, the resulting β model compares well with the derived model in the mid-corona. However, this model also agrees well with the global Pneuman–Kopp exact MHD model for streamers, which was a solution to the steady-state equations (Suess, Gary, and Nerney, 2000). The Pneuman–Kopp model has $\beta = 1.4$ at $R_s = 1.4$ and increases to 35 and 44 at 1.7 R_s. In general, $\beta \to \infty$ at the cusp of streamer models, if there is no azimuthal component for the magnetic field. Another check of the model is provided by the two cusps C1 and C2 seen in the *Yohkoh*/SXT data on 24 January 1992 and on 18 March 1999, respectively (Figure 3). These are plotted at $R = 1.23\ R_s$ and $1.25\ R_s$ with an assumed $\beta > 1$ with the upper range arbitrarily cutoff at $\beta = 5$ (Figure 3). Furthermore, SOHO/EIT data of Fe IX/Fe X at this same height (200 Mm) has a β range of 0.01–2.0, and is consistent with the model (Aschwanden *et al.*, 1999). From *Helios* observations of the Faraday rotation, Pätzold *et al.* (1987) derive the magnetic field at solar minimum between 3–10 R_s. Using their electron densities, it is seen that the β in this region is $\beta > 1$ and rises rapidly as R^3, agreeing with the trend of our model above 2 R_s. Combined WIND *in-situ* interplanetary measurements give $\beta \geq 1$, with the exception of the magnetic bubble regions where $\beta < 1$ indicating the consistency of the upper range of our model which merges with the *in-situ* data (Lepping *et al.*, 1997). This set of comparison data is consistent with $\beta > 1$ at relatively low heights ($h \sim \frac{1}{4}$–$\frac{3}{4}\ R_s$).

3. Consequences

The consequences of having the plasma β approaching unity in the mid-corona forces specific constraints on the modeling of the magnetic field, the interpretation of the solar dynamics, and rethinking the traditional paradigm of the mid-corona. We shall examine these specific points below.

3.1. Magnetic field modeling

The current magnetic field modeling derived from photospheric extrapolations is estimated to be missing a significant part (about 10–30%) of the total magnetic energy which is just the critical free energy associated with active-region eruptive events. This problem, in part, arises from not being able to specify the upper boundary conditions of the magnetic field, which leads to an ill-posed problem for magnetic field extrapolations. If the magnetic field extrapolations are limited to regions of $\beta \ll 1$, the extrapolations currently in use *must have all the appropriate boundary conditions* about a 3D domain or *make special assumptions* about these boundary conditions (Gary and Musielak, 1992; Gary, 1996). The knowledge of the complete boundary conditions does not exist. The apparent success of the current extrapolation methods results from the relative lack of sensitivity to the upper boundary conditions for which they have been employed (e.g., see the comparison of the potential field lines with coronal features given by Gary (1997) which are similar but not exact). These techniques have given a reasonable first-order approximation to the magnetic field, as seen by the quantity of papers since the early 60s (e.g., Démoulin *et al.*, 1994), but these results are good only to the first order. The apparent insensitivity to boundary conditions relates to the actual use of the extrapolations as 1st-order approximations. Only the photospheric (or at best the low chromospheric) magnetic fields can be determined from current magnetographs. The classical extrapolation problem is ill posed in that we do not have the actual needed boundary conditions.

To supplement this lack of knowledge, assumptions are made about the upper- and side-boundary conditions in all the various types of magnetic field extrapolations (e.g., Cauchy, Residual, Current Minimization, Energy Minimization, Relaxation, Variational Energy, Hydrodynamic, and Integral methods (Gary, 1990; Sakuari, 1989; Yan and Sakurai, 2000)). These methods are also limited in use due to the boundary conditions required, the physical models imposed, and/or the computer resources required. Therefore there is need for improved magnetic field modeling. The recent non-constant force-free-field solution developed by Yan and Sakurai (2000) improved the possibility of finally solving the force-free equations, but again the boundary conditions must be known and the *coronal* magnetic field must be force free everywhere. Imposing MHD methods (cf., Amari *et al.*, 1997) allows calculations of a non-linear, but again, force-free solution. Applying the boundary conditions as has been used in the last 40 years now needs to be im-

proved by stepping away from the force-free assumption and avoiding the lack of knowledge of the total boundary conditions. Even near the photosphere, Metcalf *et al.* (1995) have shown that the pressure forces are important up to 400 km above the photosphere. The paradigm that the coronal magnetic field can be constructed from a force-free magnetic field must be used in the correct context, since the force-free region is sandwiched between two regions which have $\beta > 1$.

The exact mapping of the coronal flux tubes as seen, for example in the SOHO/EIT, TRACE, and *Yohkoh*/SXT images, onto model magnetic field lines is far from satisfactory and reflects the β assumptions used in most models. For typical examples of unsatisfactory potential field line fits see Aschwanden *et al.* (1999, Figure 12) or Falconer *et al.* (2000, Figure 6). The non-force free models of Zhao and Hoeksema (1994) and Neukirch (1995) are not yet applicable to specific active regions due to their dependency on global parameters.

3.2. Minimum β magnetic field measurements ($\beta \ll 1$)

It is highly desirable to make magnetic field measurements where β is a minimum or above. The β minimum occurs $\sim$ 2 Mm above the temperature minimum at $\sim$ 0.5 Mm. The electric currents piercing through the β-minimum region will close across the coronal field lines, whereas the normal electric currents J_z that are observed in the photosphere could close in or below the temperature minimum region. Unraveling this uncertainty of the coronal currents is an important task. The NaD (588.9 nm) and Ca II (854.3 nm) vector magnetograms should be analyzed to determine if they could provide information on the electric currents closing below 0.6 and 1.4 Mm, respectively. The chromospheric Mg II–C IV magnetic measurements occur in the β-minimum region and if such vector observations could be obtained the coronal non-potential contribution from electric currents could be studied in a region dominated by magnetic pressure.

Improving the $\beta < 1$ magnetic field measurement will improve the magnetic modeling by providing a boundary condition where the magnetic field dominates and at heights that can be used as test points in the final magnetic field models.

3.3. High coronal β's at low heights

The introduction of source surface models have been used to correct the potential calculations for the upper $\beta > 1$ region. However, these source surfaces have been typically at heights of $\sim 2.5\ R_s$ and have been in the form of an infinitely thin, spherical shape. They do not account for the variation of β with height. Source surface models, if used, should have very high spatial variations to reflect the cusps over active regions and should have a variation in the vertical direction. Furthermore the plasma β can reach unity at low coronal heights, e.g., $R \sim 1.2\ R_s$, as seen by the number of low cusps observed by *Yohkoh*/SXT. This has implications on the magnetic model of the quasi-static magnetic field and the explosive events. Most extrapolation models do not consider the upper boundary conditions as a transition

to $\beta > 1$. The radial stretching analysis of Gary and Alexander (1999) has shown that this correction is important and can be incorporated into deriving non-force-free solutions for the magnetic field. Also for an active region Lites *et al.* (1995) developed a magnetostatic model which allow uniform stretching of the magnetic field in the vertical direction in order to study the topology but not to extrapolate the observed magnetic field. There are other papers that address the importance of non-magnetic forces and distorting the magnetic field. Particularly, there is a set of coronal models for CME and streamers that considers $\beta > 1$, but this set does not address correctly (nor intends to address) the β variation in the mid-corona; hence, they are not discussed here (e.g., Gibson and Low, 1998, and references therein).

3.4. PHYSICAL CONSEQUENCES

The low-lying cusps may be a physical consequence of the high-β regions in the mid-corona (quasi-static cusps) or result from an ejection event and reconnection (dynamic cusps). There are cusps that are quasi-static and β must remain high for $\sim$ 24 hours and hence are not just dynamic events. We conjecture that the dynamics of the higher TRACE observed loops might be affected by high β. These EUV images show coronal loops that are effectively evolving without influencing the global magnetic field configuration, e.g., the other coronal loops in the active region are hardly effected by the dynamical evolving loops (Schrijver *et al.*, 1999). Small magnetic changes in the photosphere or local heating can cause the β in these loops increase beyond unity at relatively low heights ($\sim 1.25\ R_s$). Pressure forces might drive some dynamic loops without having major magnetic reconnection or global magnetic field changes.

4. New Approaches

Recent work by Gary and Alexander has shown that deforming the potential field can improve the matching of field lines to coronal loops. The mathematical manipulation has been given in general for *radial* deformation by Gibson and Low (1998) and for a specific case *linear radial* deformation by Gary and Alexander (1999) and they applied their analysis to an active region. A set of deformed field lines was found to match the coronal loops using a specific radial stretch. The resulting Lorentz forces are consistent with possible non-magnetic forces to establish equilibrium. Their derived β values are given in Figure 3. The observed coronal loops are physically influenced by the upper boundary conditions and were used as a proxy of the upper boundary condition. This manipulation of the field lines has led to the idea of using all observed coronal loops at various temperatures in an active region as magnetic field line tracers, e.g., SXR/EUV images from SXT, EIT, TRACE, to provide a definite *boundary condition* for the magnetic models (see Dravins, 1974, for a similar approach). These observations can be the magnetic

field conditions to allow the inference of the coronal field topology and strengths. In such an analysis, the complex magnetic field topology of the coronal features could be investigated using a magnetic field transformation which parametrically transforms a field (and the associated field lines) to match the coronal features. The field lines can be viewed as being embedded in plastic medium and as the medium is deformed the field lines are carried along. This is similar to the frozen-in-field-line concept, but the field line movement represents a transformation (or mapping) of one magnetic field solution into another magnetic field solution. The analysis would allow the resulting magnetic field solution to match fully the magnetic field lines with SXT/EUV coronal loops. This method could calculate of the coronal magnetic field by using an ensemble of coronal EUV and SXR images which are used to define acceptable magnetic field solutions. Present extrapolations have well-known defects (as a result, in part, of the height dependency of β) and in order to improve knowledge about the coronal field an analysis program using this type of technique to determine the magnetic field, aligned and non-aligned electric currents, and the Lorentz forces in the corona associated with sinuous X-ray features seems a reasonable alternative. This alternate approach would account for (1) the actual β changes with height, as given in Figure 3; (2) the unknown boundary conditions on the field and velocities; and (3) the non-force-free effects in the two $\beta > 1$ regions which sandwich the mid-corona.

Acknowledgements

Part of this work was supported by the NASA's Office of Space Science. I would like to thank R. Moore, D. Rabin, and S. Suess for their helpful comments and suggestions that improved this paper and the referee for helping to greatly clarify the manuscript.

References

Allen, C. W.: 1973, *Astrophysical Quantities*, Athlone Press, London, p. 161.
Altschuler, M. D. and Newkirk, G.: 1969, *Solar Phys.* **9**, 131.
Amari, T., Aly, J. J., Luciani, J. F., Boulmezaoud, T. Z., and Mikić, Z.: 1997, *Solar Phys.* **174**, 129.
Aschwanden, M. K., Schrijver, C. J., and Alexander, D.: 2001, *Astrophys. J.* **550**, 1036.
Aschwanden, M. J., Newmark, J. S., Delaboudinière, J.-P., Neupert, W. M., Klimchuk, J. A., Gary, G. A., Portier-Fozzani, F., and Zucker, A.: 1999, *Astrophys. J.* **515**, 842.
Berton, R.: 2000, *Astron. Astrophys.* **356**, 301.
Bruls, J. H. M. J., Lites, B. W., and Murphy, G. A.: 1991, in L. J. November (ed.), *Solar Polarimetry*, NSO/Sacramento Peak Summer Workshop XI, Sunspot, NM, p. 444.
Darvins, D.: 1974, *Solar Phys.* **37**, 323.
Démoulin, P., Mandrini, C. H., Rovira M. G., Hénoux, J. C., and Machado, M. E.: 1994, *Solar Phys.* **150**, 221.
Dulk, G. A. and McLean, D. J.: 1978, *Solar Phys.* **57**, 279.

Falconer, D. A., Gary, G. A., Moore, R. L., and Porter, J. G.: 2000, *Astrophys. J.* **528**, 1004.
Fontenla, J. M., Avrett, E. H., and Loeser, R.: 1990, *Astrophys. J.* **355**, 700.
Gary, G. A.: 1990, *Mem. Soc. Astron. It.* **61**, 457.
Gary, G. A.: 1996, *Solar Phys.* **163**, 43.
Gary, G. A.: 1997, *Solar Phys.* **174**, 241.
Gary, G. A. and Alexander, D.: 1999, *Solar Phys.* **186**, 123.
Gary, G. A. and Musielak, Z. E.: 1992, *Astrophys. J.* **392**, 722.
Gibson, S. E. and Low, B. C.: 1998, *Astrophys. J.* **493**, 460.
Harvey, J. W.: 1969, Ph.D. Thesis, University of Colorado, Boulder.
Hagyard, M. J., Teuber, D., West, E. A., Tandberg-Hanssen, E., Henze, W. Jr., Beckers, J. M., Bruner, M., Hyder, C. L., and Woodgate, B. E.: 1983, *Solar Phys.* **84**, 13.
Hiei, E. and Hundhausen, A. J.: 1996, in Y. Uchida, T. Kosugi, and H. S. Hudson (eds.), *Magneto-dynamic Phenomena in the Solar Atmosphere - Prototypes of Stellar Magnetic Activity*, Kluwer Academic Publishers, Dordrecht, Holland, p. 125.
Kano, R. and Tsuneta, S.: 1995, *Astrophys. J.* **454**, 934.
Kopp, G. and Rabin, D.: 1992, *Solar Phys.* **141**, 253.
Lee, J., White, S. M., Gopalswamy, and Kundu, M. R.: 1997, *Solar Phys.* **174**, 175.
Lepping, R. P., Burlaga, L. F., Szabo, A., Ogilive, K. W., Mish, W. H., Vassiliadis, D., Lazarus, A. J., Steinberg, J. T., Farrugia, C. J., Janoo, L., and Mariani, F.: 1997, *J. Geophys. Res.* **102**, 14049.
Lin, H., Penn, M. J., and Tomczyk, S: 2000, *Astrophys. J.* **541**, L83.
Lites, B. W., Low, B. C., Martínez Pillet, V., Seagraves, P., Skumanich, A., Frank, Z. A., Shine, R. A., and Tsuneta, S.: 1995, *Astrophys. J.* **446**, 877.
McClymont, A. N. and Mikic, Z.: 1994, *Astrophys. J.* **422**, 899.
McKenzie, D. E. and Hudson, H. S.: 1999, *Astrophys. J.* **519**, L93.
Metcalf, T. R., Jiao, L, McClymont, A. N., Canfield, R. C., and Uitenbroek, H.: 1995, *Astrophys. J.* **439**, 474.
Moore, R. L., Sterling, A. C., Hudson, H. S., and Lemen, J. R.: 2001, *Astrophys. J.* **552**, 883.
Neukirch, T.: 1995, *Astron. Astrophys.* **301**, 628.
Pätzold, M., Bird, M. K., Volland, H., Levy, G. S., Siedel, B. L., and Stelzried, C. T.: 1987, *Solar Phys.* **109**, 91.
Pneuman, G. W. and Kopp, R. A.: 1971, *Solar Phys.* **18**, 258.
Rabin, D.: 1992, *Astrophys. J.* **391**, 832.
Rosner, R., Tucker, W., and Vaiana, G.: 1978, *Astrophys. J.* **220**, 643 (RTV).
Rüedi, I., Solanki, S. K., Livingston, W., and Stenflo, J. O.: 1992, *Astron. Astrophys.* **263**, 323.
Sakurai, T.: 1989, *Space Sci. Rev.* **51**, 1.
Socas-Navarro, H., Trujillo Bueno, J., and Ruiz Cobo, B.: 2000, *Astrophys. J.* **530**, 977.
Schatten, K. H., Wilcox, J. M., and Ness, N. F.: 1969, *Solar Phys.* **6**, 442.
Schrijver, C. J., Title, A. M., Berger, T. E., Fletcher, L., Hurlburt, N. E., Nightingale, R., Shine, R. A., Tarbell, T. D., Wolfson, J., Golub, L., Bookbinder, J. A., Deluca, E. E., McMullen, R. A., Warren, H. P., Kankelborg, C. C., Handy, B. N., and de Pontieu, B.: 1999, *Solar Phys.* **187**, 261.
Strong, K. T.: 1994, in S. Enome and T. Hirayama (eds.), *New Look At the Sun with Emphasis on Advanced Observations of Coronal Dynamics and Flares*, Proceedings of Kofu Symposium, NRO Report No. 360. Nagano, Japan, pp. 53–56.
Suess, S. T., Gary, G. A., and Nerney, S. F.: 2000, in S. R. Habbal, R. Esser, J. V. Hollweg, and P. A. Isenberg (eds.), *Solar Wind Nine* (CP-471), The American Institute of Physics, 247.
Vernazza, J. E., Avrett, E. H., and Loeser, R.: 1981, *Astrophys. J. Suppl. Ser.* **45**, 635.
Yan, Y. and Sakurai, T.: 2000, *Solar Phys.* **195**, 89.
Yokoyama, T., Akita, K., Morimoto, T., Inoue, K., and Newmark, J.: 2001, *Astrophys. J.* **546**, L69.
Yoshida, T. and Tsuneta, S.: 1996, *Astrophys. J.* **459**, 342.
Zhao, X. and Hoeksema, J. T.: 1994, *Solar Phys.* **151**, 91.